

Cover Page



Universiteit Leiden



The handle <http://hdl.handle.net/1887/30224> holds various files of this Leiden University dissertation.

Author: Neshati, Zeinab

Title: Cellular models and viral vectors for skeletal and cardiac muscle research

Issue Date: 2014-12-23

Chapter 3

Evaluating the Biodegradability of Gelatin/Siloxane/ Hydroxyapatite (GS-Hyd) Complex *in vivo* and its Ability for Adhesion and Proliferation of Rat Bone Marrow Mesenchymal Stem Cells

Zeinab Neshati, Ahmad Reza Bahrami, Hossein Eshtiagh-Hosseini,
Maryam M. Matin, Mohammad Reza Housaindokht, Taymaz Tabari,
Mohammad Amin Edalatmanesh

Cytotechnology. 2012;64:485-495.

Abstract

Recent studies have shown that the use of biomaterials and new biodegradable scaffolds for repair or regeneration of damaged tissues is of vital importance. Scaffolds used in tissue engineering should be biodegradable materials with three-dimensional structures, which can guide the growth and differentiation of the cells. They also should possess physical, chemical and biological properties that allow efficient supply of the cells to target tissues and have proper porosity along with minimal toxic effects. In this study, Gelatin/Siloxane/Hydroxyapatite (GS-Hyd) scaffold was synthesized and its morphology, *in vivo* biodegradability, cytotoxic effects and ability for cell adhesion were investigated using mesenchymal stem cells (MSCs). The cells were treated with different volumes of the scaffold suspension to evaluate its cytotoxic effects. The MSCs were also seeded on scaffolds and cultured for 2 weeks for assessing the scaffold's ability to promote cell adhesion and proliferation. To check the biodegradability of the GS-Hyd complex *in vivo*, scaffolds were implanted into the thigh muscle, testicle, and liver of rats and analyzed at 3, 7, 16 and 21 days after implantation by scanning electron microscopy (SEM) and weighing. The viability studies showed that the GS-Hyd scaffold exerted no cytotoxic effects on the cells and that the MSCs readily adhered to the scaffold with the expansion of their elongations and the formation of colonies. The rate of scaffold degradation as assessed by weighing was significant within each group at some time points along with significant differences between different tissues at the same time point. SEM micrographs indicated obvious changes at the surface of the scaffold particles and in the diameter of their pores through different stages of implantation. At 21 days after implantation the loss of scaffold was highest in the muscle and lowest in the liver.

Keywords

Tissue engineering, Gelatin/Siloxane/Hydroxyapatite scaffold, Biodegradability, Mesenchymal stem cells, Tissue regeneration

Introduction

Several strategies are employed to compensate for the loss of functional tissue in incurable diseases including cell, tissue and organ transplantation, surgical reconstruction, synthetic prostheses, and medical devices. However, each of these treatments, suffers from some problems or limitations. For example, organ transplantation is limited by donor shortage and usually requires lifelong consumption of immunosuppressive drugs, which may cause severe complications.¹ Although the other therapies are not limited by supply, they also have limitations. For example, synthetic prostheses and medical devices are generally not able to replace all the functions of damaged, diseased or lost tissue.

Tissue engineering has emerged as an expanding approach to address these problems and is now a major component of regenerative medicine.²⁻⁴ By combining engineering principles with material science and molecular biology, investigators seek to create novel constructs that will fully integrate into the host system and restore function of the lost tissues.⁵ The general principle of cell-based tissue engineering involves combining living cells with a natural/synthetic support or scaffold.⁶ The main roles of the porous three-dimensional (3D) scaffolds are to give structural support and to provide an optimal environment for the cells contained inside. Following their isolation from healthy tissue and *in vitro* expansion, the cells should adhere to the scaffold in all three dimensions, proliferate, differentiate and secrete their own extracellular matrices (ECMs), gradually replacing the scaffold.^{4,7} Therefore, in addition to permitting cell adhesion, promoting cell growth, and allowing retention of differentiated cell functions, the scaffold should be biocompatible, biodegradable, highly porous with a large surface to volume ratio, able to facilitate the necessary crosstalk with surrounding cells, mechanically strong, and capable of being formed into desired shapes with considerable stability.⁸⁻¹¹

A variety of hydrolytically degradable polymers have been developed for scaffold applications in tissue engineering. The majority of these polymers are composed of linear aliphatic polyesters with a high molecular weight and their copolymers. These materials often possess mechanical properties best suited for engineering of hard tissues.¹²⁻¹⁷ However, for engineering of soft tissues, flexible scaffolds are desirable.¹⁸ The biomaterials used to construct these porous scaffolds include synthetic biodegradable polymers such as polyglycolic acid (PGA), polylactic acid

(PLA), and their copolymer poly DL-lactic-co-glycolic acid (PLGA), and also polymers derived from natural materials such as collagen and inorganic hydroxyapatite.^{17,19,20} In this study, the GS-Hyd complex was synthesized by combining Gelatin, Siloxane and hydroxyapatite as will be explained below. Hydroxyapatite, mainly in a carbonated form, is the major inorganic constituent of natural bone.^{21,22} Synthetically made hydroxyapatite ($\text{Ca}_5(\text{PO}_4)_3(\text{OH})$) has long been used in medicine and dentistry due to its ability to chemically attach to bone. It has been used as a hard tissue replacement, usually in the form of fillers (pastes, powders), or as a bioactive agent in polymer composites.²¹ Pure, stoichiometrical hydroxyapatite is the least degradable form of calcium phosphate.²³ Often, other more soluble mineral phases of apatite are preferred as bone-substitute materials in order to combine calcium-ion release properties with chemical stability of the support.²⁴⁻²⁶ Amongst those are non-stoichiometrical hydroxyapatite (calcium-deficient hydroxyapatite (CDHA)), β -tricalcium phosphate (β -TCP), octacalcium phosphate (OCP), or biphasic hydroxyapatite (BCP, various hydroxyapatite/ β -TCP ratios).²⁴⁻²⁷ A number of synthetic routes towards the preparation of biologically active calcium phosphates, including different templating approaches, have been reported.²⁸⁻³² The presence of silica in many biocompatible and bioactive materials has generally been shown to improve their bioactivity.^{33,34} Studies show that introduced or already present silanol groups provide good nucleation sites for hydroxyapatite.³⁵ Silica is also one of the vital components in bioglass, but is also used in polymer composites and thin films.³⁶⁻⁴⁰ In addition, natural polymers like collagen, gelatin and chitosan are osteoconductive and biodegradable components that have been used in fabrication of scaffold materials for tissue engineering.^{41,42} Thus, combining these natural polymers with the inorganic species mentioned above may yield biodegradable and bioactive scaffolds for tissue engineering.⁴³ Scaffolds are normally analyzed by scanning electron microscopy (SEM) for their pore sizes, internal connections, and physical appearances. In the scaffold biodegradability process, both *in vitro* and *in vivo*, the pore diameters and volume of the scaffolds can be determined by SEM.⁴⁴

Development of a viable construct also requires a suitable supply of cells that are ideally non-immunogenic, highly proliferative, easy to harvest and have the ability to differentiate into a variety of cell types with specialized functions.⁴⁵⁻⁴⁷ Possible candidates for such purpose are bone marrow-derived mesenchymal stem cells (BM-MSCs), which have the potential to differentiate into various types of

mesenchymal tissues, including osteoblasts, chondroblasts, myoblasts and fibroblasts.⁴⁸ They are present in large quantities in animal and human bodies, can be easily obtained, and greatly expanded *in vitro*.^{49,50} Moreover, BM-MSCs are hypoimmunogenic cells that do not induce immune system response⁵¹ and have been successfully used to promote repair of different connective tissues, such as bone,⁵² cartilage,⁵³ tendon,⁵⁴ and ligament.⁵⁵ We have also shown in our previous studies, the capacity of MSCs to differentiate into insulin-producing and neural cells in animal models of diabetes and Huntington's disease, respectively.^{56,57}

In this study, the GS-Hyd complex was synthesized and the three main questions relevant for its use as scaffold were studied, *i.e.* (a) whether it affects cell viability, (b) whether it supports the cell adhesion and proliferation, and (c) whether it is biodegradable *in vivo*.

Materials and Methods

Scaffold preparation

Starting materials used in this investigation for synthesis of the scaffold, including analytical grade calcium nitrate tetrahydrate ($\text{Ca}(\text{NO}_3)_2 \cdot 4\text{H}_2\text{O}$), phosphoric pentoxide (P_2O_5) and tetraethoxyorthosilicate (TEOS) were purchased from Aldrich, Germany. All materials were used as received, without further purification.

Solutions of P_2O_5 (0.5 mol/L (absolute ethanol)) and solution of $\text{Ca}(\text{NO}_3)_2 \cdot 4\text{H}_2\text{O}$ (1.67 mol/L (absolute ethanol)) were prepared. They were mixed together in a Ca/P molar ratio of 1.67 to generate a calcium phosphate precursor solution. The mixture was then continuously stirred about 10 min at ambient temperature, followed by heating in a water bath at 60 °C for 1 h. A 12.5% solution of gelatin was prepared by dissolution in 0.1 M HCL. Addition of appropriate amount of calcium phosphate precursor solution to the gelatin solution resulted in the hybrid solution. After this ripening process, 5 ml TEOS was added to the mixture under continuous stirring, corresponding to 60% SiO_2 in the final SiO_2 /calcium phosphate material. The obtained gel was aged at room temperature for 20 h before calcination at 550 °C for 8 h (heating rate 1 K min⁻¹), to remove all organics from the material.

Animals

In all experiments, male Wistar rats with an average weight of 250 g were used. Rats were kept at standard conditions and subjected to 12-hour cycles of light and darkness.

BM-MSCs extraction and culture

Bone marrow (BM) was obtained from the femurs and tibias of rats. BM was flushed into Dulbecco's Modified Eagle's Medium (DMEM, Gibco, Scotland) supplemented with 15% fetal bovine serum (FBS, Gibco, Scotland), 100 units/ml penicillin, and 100 µg/ml streptomycin (Biosera, UK) and incubated in a humidified incubator at 37 °C with 5% CO₂. When cultures reached about 80% confluency, they were washed with phosphate-buffered saline (PBS) followed by a 5 min incubation with 0.05% trypsin solution at 37 °C. Cells were split weekly at a ratio of 1:3.

Cytotoxicity assay of GS-Hyd

5×10^3 of MSCs at passage 3 were seeded in each well of 96-well microplates and incubated for 48 h at 37 °C. Then, 80 mg of powdered scaffold was dissolved in 2 ml DMEM supplemented with 15% FBS, and cells were exposed to various volumes of the resulting GS-Hyd suspension (2, 4, 8, 16, 32, 64, 128 and 200 µl), with three repeats for each volume. Cells cultured in DMEM supplemented with 15% FBS without GS-Hyd were used as controls. Total volume in each well was 200 µl. The effect of GS-Hyd on cell viability was measured by 3-[4,5-dimethylthiazol-2-yl]-2,5-diphenyl tetrazolium bromide (MTT, Merck, Germany) staining. MTT assay was performed after 48 h of treatment. Cells in each well were incubated in 20 µl MTT solution (5 mg/ml MTT in PBS) for 4 h at 37 °C. The intense purple-colored formazan derivative formed via cell metabolism was then dissolved in 200 µl/well dimethylsulfoxide (DMSO, Merck, Germany) and the absorbance was measured at 570 nm by ELISA plate reader (Awareness Technology, USA). The cell viability in the presence of different volumes of GS-Hyd was calculated using the following formula: absorbance of each treated well/mean absorbance of control wells \times 100. The average cell viability for each volume of GS-Hyd was then calculated and presented in a graph using Microsoft Excel.

Seeding of MSCs on GS-Hyd scaffold

MSCs at passage 3 were trypsinized and suspended in DMEM followed by counting with a hemocytometer. The cell suspension was then centrifuged at $67.2 \times g$ for 5 min and the pellet was resuspended in DMEM, supplemented with 15% FBS, 100 units/ml penicillin and 100 $\mu\text{g/ml}$ streptomycin at a concentration of 10^7 cells/ml. After the scaffold had been cut into small pieces (5 mm \times 3 mm) and sterilized by autoclaving, the GS-Hyd pieces were placed on agarose-coated (1% agarose in sterile H_2O) 6-well culture plates (3 scaffolds/well), and divided into two test and control groups. The scaffolds received 100 μl medium without cells served as controls, while each scaffold in the test group was seeded with 10^6 cells in 100 μl medium. The scaffolds were incubated for 4 h in a humidified atmosphere at 37 $^\circ\text{C}$ and 5% CO_2 to allow cell attachment. Then 3 ml of the medium was added to each well and the scaffolds were incubated for 2 weeks. The medium was replaced every 2–3 days. On days 1, 7 and 14 the scaffolds were collected to be evaluated for cell attachment by SEM.

Preparation of the cell-seeded scaffolds for SEM

Scaffolds were fixed in 3% buffered glutaraldehyde for 24 h, dehydrated with a graded ethanol series, and dried. The dried samples were mounted on aluminum stubs and sputter-coated (SC7620 sputter coater) with gold for 2 min. SEM was used to take micrographs of the samples. The GS-Hyd scaffold was characterized mainly by Fourier transform infrared spectroscopy (FTIR), differential thermal analysis (DTA), and transmission electron microscopy (TEM). Simultaneous DTAs were carried out in the range of 20–1,000 $^\circ\text{C}$ in a Netzsch STA 409 $^\circ\text{C}$ instrument under air and at the rate of 10 $^\circ\text{C}/\text{min}$.

Preparation of scaffold for in vivo implantation

Another series of scaffolds were cut in small segments (5 mm \times 3 mm), submerged in 70% ethanol for 30 min, and washed with PBS. The scaffolds were then kept in PBS until the start of the surgery. Scaffolds were polished on the edges to ensure that they were not sharp. The weight of the scaffolds was recorded before the ethanol wash and placement in the PBS.

Preparation of animals for implantation surgery

All tests and experimental protocols were approved by the Ethics Committee of Ferdowsi University of Mashhad. Animals were anesthetized by a mixture of ketamine hydrochloride (100 mg/kg) and xylazine (5 mg/kg). The regions for the surgery (thigh muscle, testicles and liver) were sterilized with 70% ethanol after shaving.

For implantation of the scaffold in thigh muscle, a deep incision of 1 cm along the length of the muscle was made with a scalpel. Next, tampons were used to stop bleeding. If bleeding persisted, the site of incision was cauterized. The scaffold was then gently lowered in between the muscle fibers. After this step, the muscle was stitched layer by layer towards the surface. To implant the scaffold in a testicle, an incision was made in the scrotum. One of the testicles was exposed, and without applying too much pressure to the testicle, a hole with the exact size of the scaffold was made by scalpel. The scaffold was subsequently placed in the testicle and the testis and scrotum were stitched. For implantation of the scaffold in the liver, a deep incision of about 1 cm was made below the right side of the rib cage, until the visceral peritoneum of the liver appeared. Then, a small hole was made in the liver and the scaffold was placed inside and the peritoneum layers and skin were stitched separately.

At the end of each surgical procedure, the stitched tissues were sterilized with betadine and Lidocaine gel was applied to numb them. As extra measure against possible infections, every rat was injected intraperitoneally with 5,000 unit/kg penicillin. After surgery, the animals were moved to a recovery cage to regain their consciousness in a warm blanket. The conditions of the rats was monitored by checking their breathing, taking their pulse and measuring their body temperature. When the rats showed normal vital signs and movements, they were returned to their original cage.

Degradation assay of GS-Hyd

To analyze the degradability of the scaffold by weight changes, 3 rats per scaffold implantation site were anaesthetized at 3, 7, 16, and 21 days after implantation, and the scaffolds were removed from their bodies. On these days, the anatomical condition and histology of the surgery site were carefully studied. When each scaffold was removed from the body, it was immediately washed with normal saline

to remove blood and extra tissues. Each scaffold was placed into a separate test tube with specific identification number. The test tubes were then placed in oven at 50 °C for 30 min. After the scaffolds were completely dried, they were weighed with a sensitive electronic scale. The weight of the scaffolds after explantation were compared to their weight prior to surgery and the percentile weight loss was recorded. To check the rate of degradation using SEM, scaffold samples from each part of the body (thigh muscle, testicle and liver) were prepared using the same procedure. The number of connections between the pores of the scaffolds and the diameter and dispersion of the pores were assessed as indicators of scaffold degradation.

Statistical analysis

Data were analyzed using one way ANOVA. All group comparisons were analyzed using Tukey's *post hoc* test to determine which groups were significantly different from each other. *P* values ≤ 0.05 were considered to indicate statistical significance.

Results

Chemical and structural characteristics of GS-Hyd scaffold

GS-Hyd scaffold showed sharp absorption bands in FTIR that were attributed to hydroxyapatite: 3th vibration of PO_4^{3-} ($\nu_3\text{PO}_4^{3-}$) at 1,045–1,092 cm^{-1} and $\nu_2\text{PO}_4^{3-}$ at 474 cm^{-1} , $\nu_1\text{PO}_4^{3-}$ symmetric stretch at 963 cm^{-1} , $\nu_4\text{PO}_4^{3-}$ bending at 602 and 572 cm^{-1} . The broad absorption bands at 3,100–3,600 cm^{-1} belonged to OH stretching absorption bands. Extensive absorption around 630 cm^{-1} (structural OH stretching) was attributed to hydroxyapatite's crystalline structure. The silica layer showed weak absorption bands around 800 cm^{-1} corresponding to the Si–O–Si bonds. Some of the silica absorption bands were hard to identify due to stronger, overlapping absorption bands from hydroxyapatite. That is especially true in the area around 1,185 and at 1,000–1,085 cm^{-1} where the Si–O–Si vibration bands usually are the strongest, but also around 960 cm^{-1} where the Si–OH silanol groups absorb (data not shown).

Figure 1 shows the thermogram corresponding to simultaneous DTA at 70 °C/24 h. In the DTA curve of the precursor GS-Hyd scaffold (Figure 1), after dried in 70 °C, exothermic peaks assignable to organic combustion are visible. In order to

discard the presence of water occluded in the exhaustively dried sample after 150 °C, a simultaneous DTA was carried out due to its considerably higher sensibility. DTA showed the combustion peak of residual gelatin at 320 °C, and a very low peak at 590 °C. It can thus be concluded that the microporosity observed after calcination is originated by the elimination of gelatin macromolecules forming microdomains in the silica matrix.

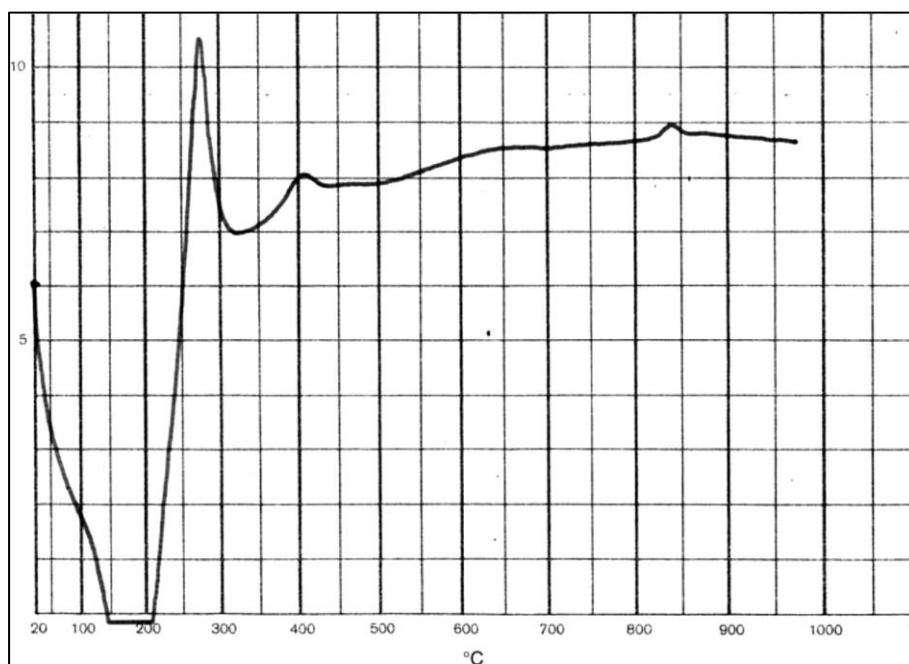


Figure 1. DTA thermogram of GS-Hyd.

The simple one-pot synthesis method resulted in a fairly homogeneous distribution of the mesoporous silica throughout the apatite crystal surface as demonstrated by the TEM micrograph (Figure 2). The crystalline size of the GS-Hyd scaffold is about 50 nm. This could be the reason for even distribution of hydroxyapatite over the surface of silica matrix. On the other hand, the material lacks a well-pronounced mesoporous long-range order in the silica layer.

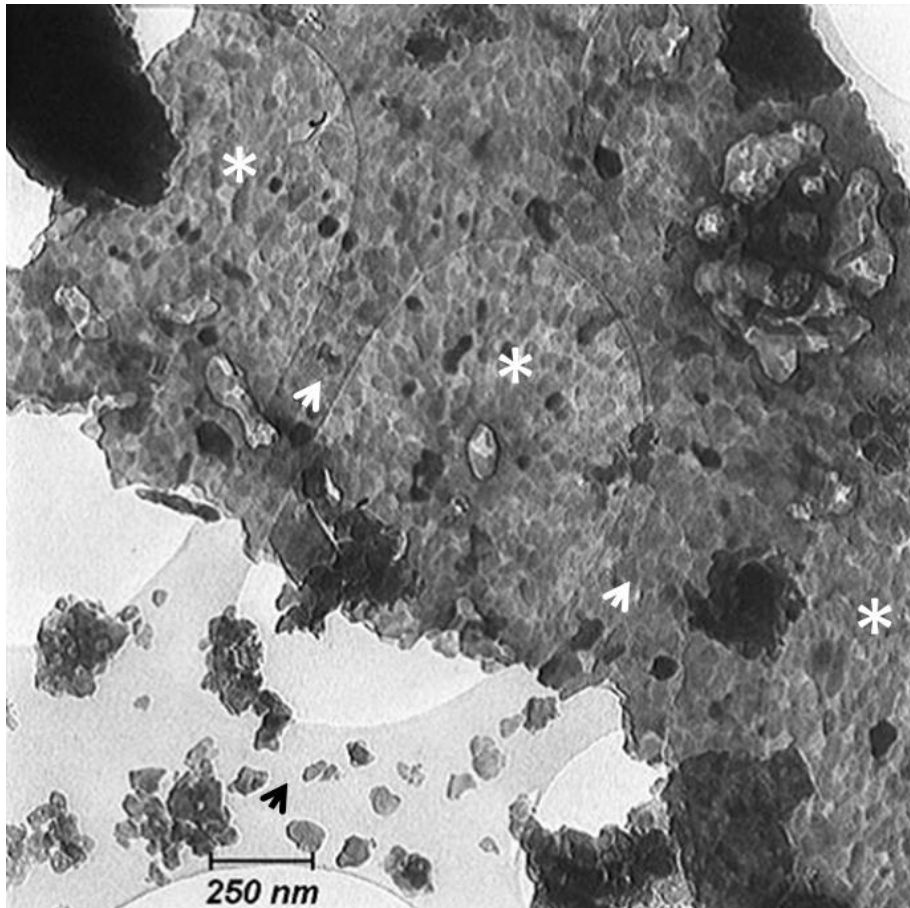


Figure 2. TEM image of GS-Hyd showing the great growth of hydroxyapatite (arrows) and the deposition of silica among its pores (asterisks).

Homing of MSCs in GS-Hyd scaffolds

As mentioned previously, to investigate the biocompatibility of the GS-Hyd complex, scaffolds were seeded with 10^6 BM-MSCs and scaffolds without cells served as negative controls (Figure 3). On days 1, 7 and 14 after cell seeding, scaffolds were collected to be evaluated for cell attachment and proliferation by SEM. Cells were round shaped at the time of seeding (not shown) but adhered to the scaffold, expanded their elongations and obtained a fibroblast-like appearance within 24 h (Figure 4). Moreover, during their cultivation on scaffolds, the BM-MSCs proliferated resulting in the formation of colonies (Figure 5).

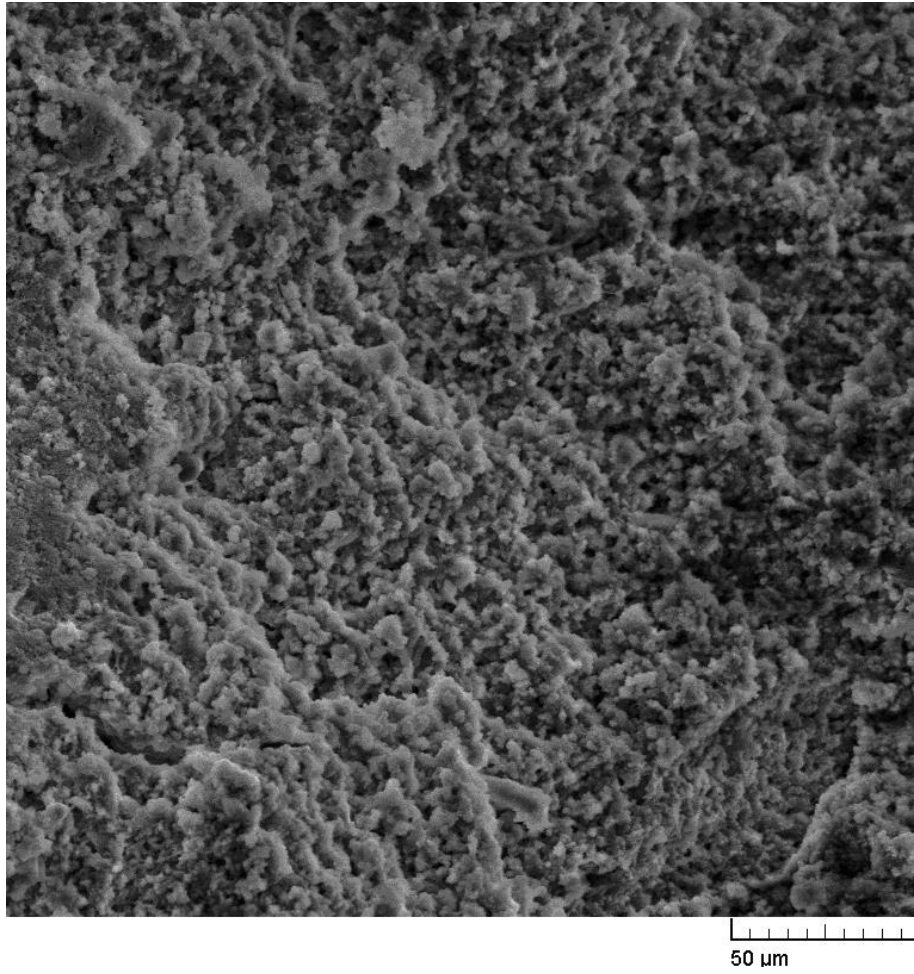


Figure 3. SEM micrograph showing the morphology of the GS-Hyd scaffold without cells.

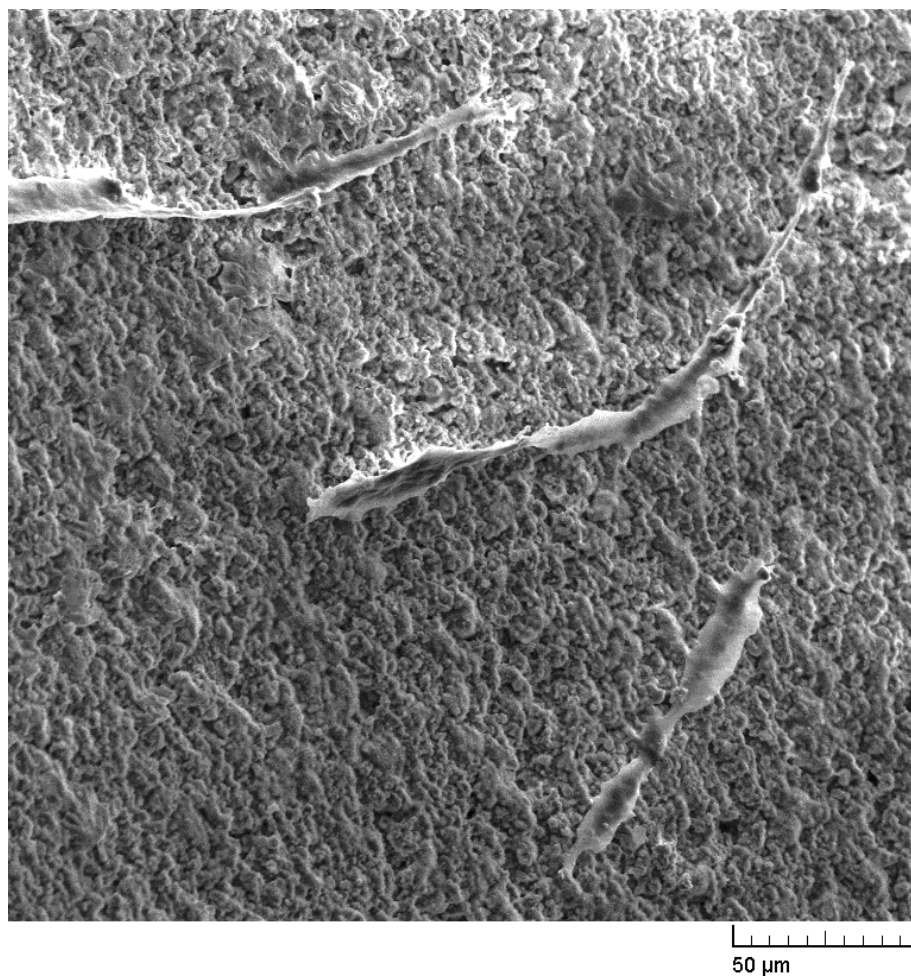


Figure 4. SEM micrograph showing scattered distribution of MSCs on the surface of the scaffold 24 h after cell seeding.

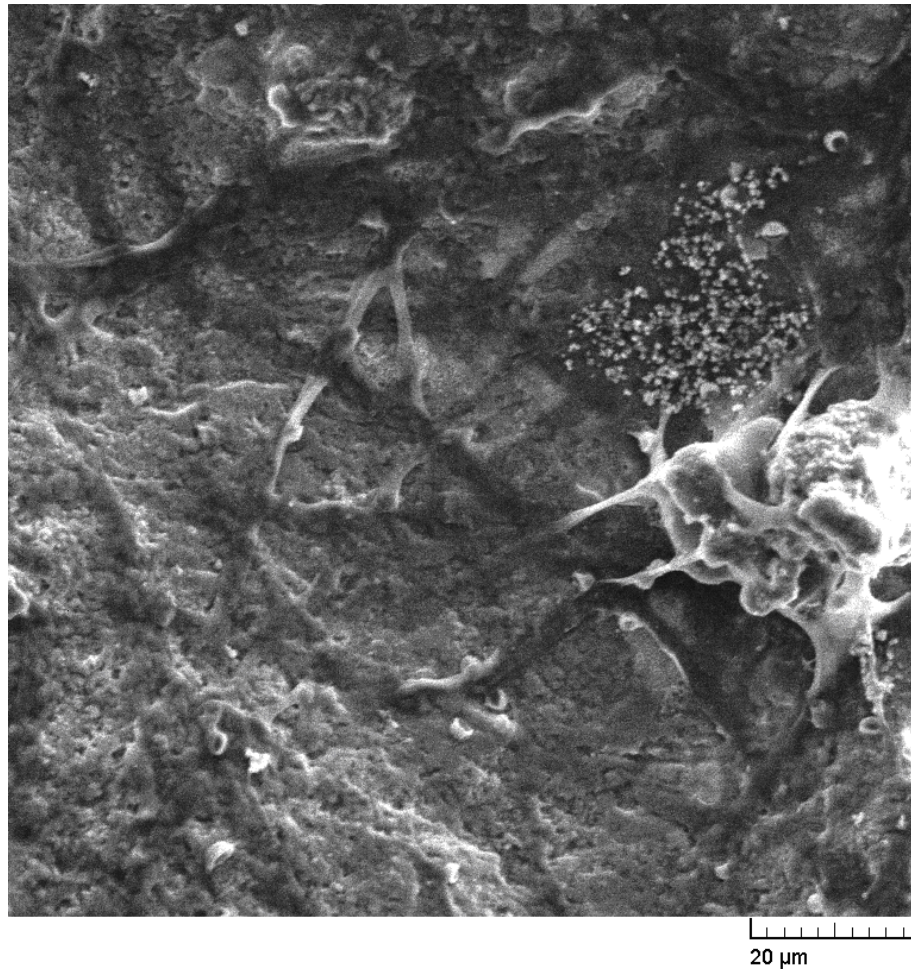


Figure 5. SEM micrograph showing MSC proliferation and colony formation on the scaffold, 7 days after cell seeding.

Cytotoxicity of GS-Hyd scaffold

The MTT assay is a colorimetric method for measuring the activity of enzymes that reduce the colorless MTT to purple colored formazan dyes. Its main application is assessment of the viability and the proliferation of cells. It can also be used to determine cytotoxicity of potential medicinal agents and toxic materials, since those agents would stimulate or inhibit cell viability and growth.

The MTT assay showed that GS-Hyd has no detectable cytotoxic effects on the cells up to concentration of 25.6 mg/ml (128 μl). Cell viability decreased only at the highest amount of GS-Hyd (200 μl) as shown in Figure 6.

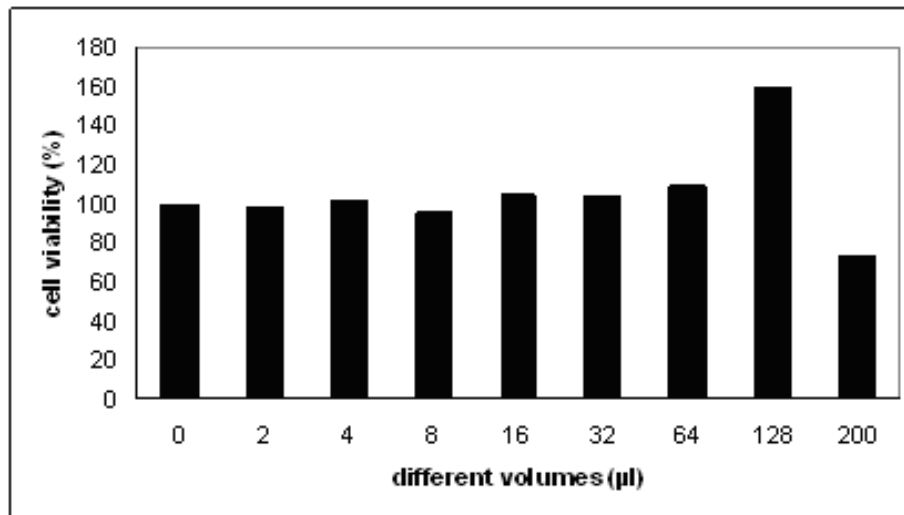


Figure 6. Effects of different volumes of GS-Hyd suspension on the viability of MSCs as measured by MTT assay.

In vivo degradability of GS-Hyd scaffold

The degradation rate of scaffolds implanted at different sites was determined by weighing them following their explantation at 3, 7, 16 and 21 days after transplantation. The weight reduction at day 3 significantly differed from those at day 16 and 21 for scaffolds in all three anatomical sites, but the differences between other days were not significant. At day 7, the differences between thigh muscle and liver ($P < 0.0001$) and between liver and testis were significant ($P < 0.001$), but there was no significant difference between thigh muscle and testicle. The differences between different tissues at other time points were significant (Figure 7).

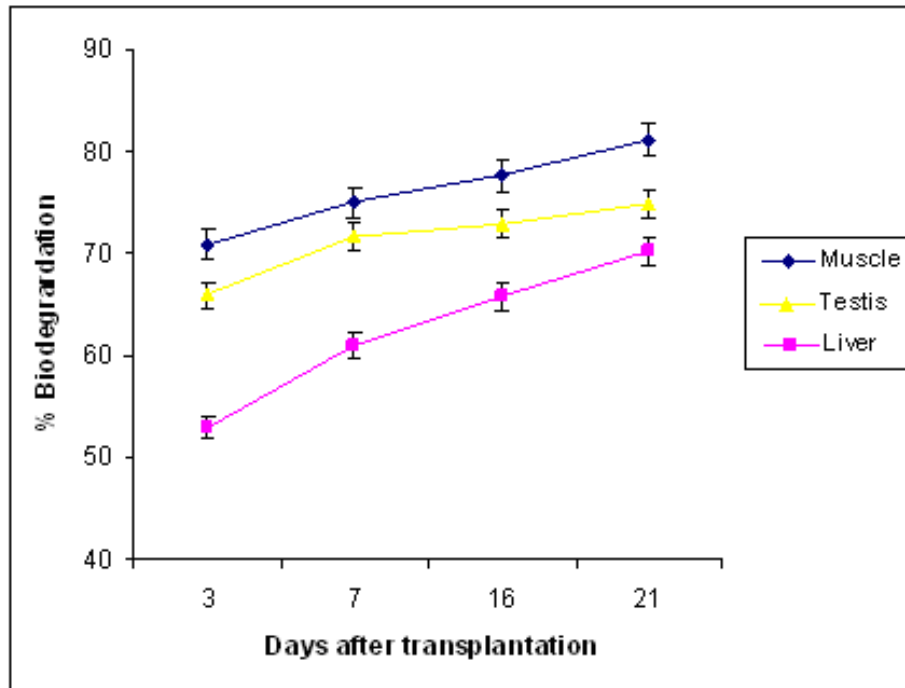


Figure 7. Comparison of the rate of scaffold degradation in various anatomical positions on different days after implantation. There are significant differences in each group during the time period and between groups at the same time point. Vertical bars indicate means \pm SEM in rats of each group at each measurement ($n = 3$, $P \leq 0.05$).

Structural changes of GS-Hyd scaffolds following in vivo implantation

Transplanted GS-Hyd particles underwent clear time-dependent morphological changes on their surface as evinced by SEM micrographs of scaffolds explanted at different times after implantation (Figure 8). These changes in surface structure were accompanied by an increase in diameter of the pores. Consistent with the results presented in Figure 7, degradation of the GS-Hyd scaffold at 21 days post implantation was highest in the thigh and lowest in the liver (Figure 8, B–D).

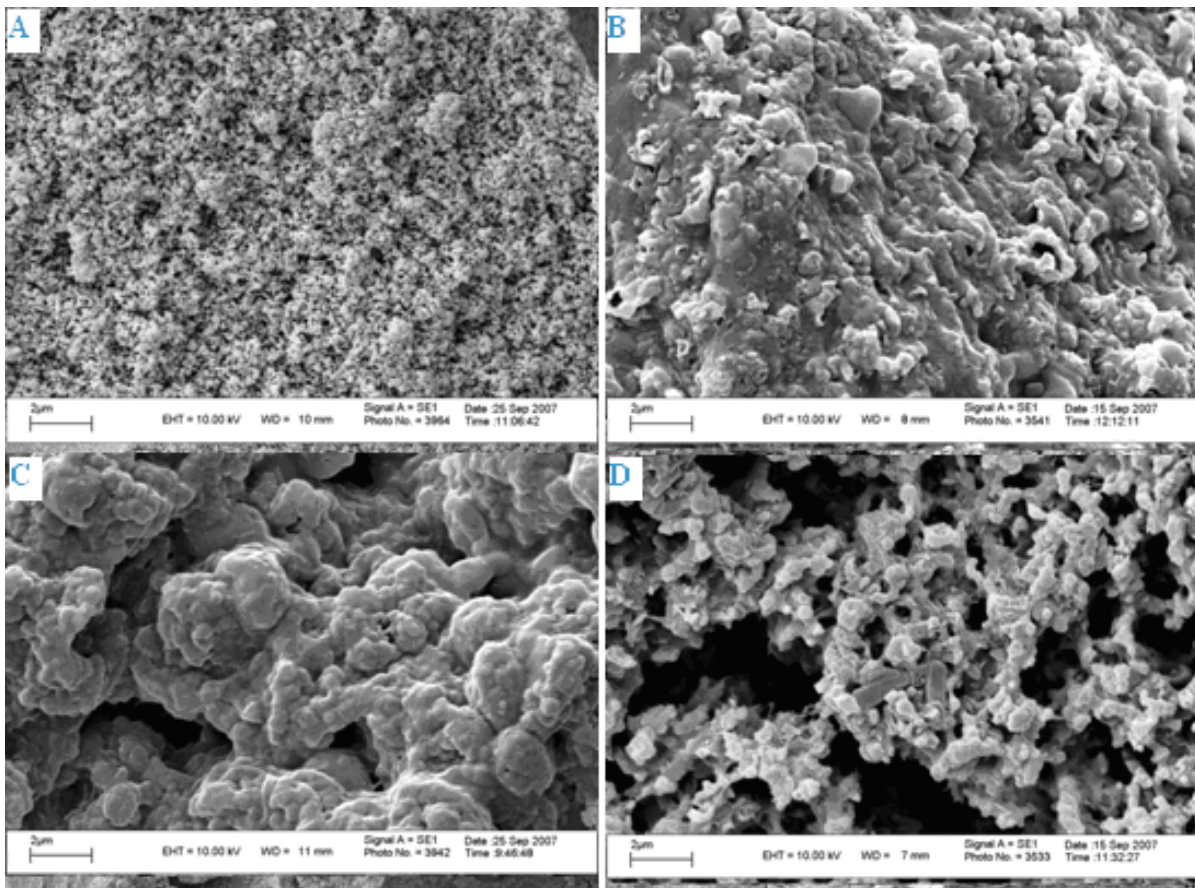


Figure 8. SEM micrographs of the scaffold before (A) and after (B–D) implantation in the liver (B), testicle (C) and thigh muscle (D).

Discussion

One of the main problems in cell therapy is homing of the cells and their maintenance in desired areas, which may be overcome by growing the cells on scaffolds followed by their transplantation at the target sites. The major concerns in applying external scaffolds in tissue engineering are severe immune responses, persistence to degradation, and unexpected side effects. As mentioned before (1) the specific material composition of the scaffold and (2) the cell source are two important elements, which can substantially affect the outcome of tissue engineering.⁵ Application of biodegradable materials is a vital factor in tissue engineering.⁵⁸ Scaffolds should also be mechanically strong, capable of being formed into desired shapes, non-cytotoxic and highly porous for permitting cell adhesion and growth.^{8,9} Development of such an efficient scaffold also involves a

suitable supply of cells such as MSCs, which, due to their specific properties, are attractive candidates for clinical applications. For example, Liu and colleagues cultured anterior cruciate ligament fibroblasts (ACLFs) and BM-MSCs on combined silk scaffolds to determine which of these two cell types would be best suited for ligament tissue engineering applications. Their preliminary results demonstrated that BM-MSCs are superior to ACLFs, with respect to cell proliferation and *in vivo* survival.⁵⁹ Moreover, the safety of MSCs for *in vivo* applications has been shown by numerous studies in animals and humans and the clinical use of MSCs is not associated with major ethical concerns unlike the therapeutic use of embryonic stem cells (ESCs). Although some studies have shown a promotion of tumor growth and metastasis after implantation of MSCs, tumor induction is mostly described for embryonic stem cells (ESCs).^{60,61}

Cell adhesion to substrate is known to affect cell behavior and function in both natural and engineered tissues and plays a key role in morphogenesis and organogenesis.^{62,63} In this study, we used MSCs as candidate stem cells and GS-Hyd scaffold as a cell carrier for adhesion and proliferation of the cells *in vitro*. GS-Hyd is a 3D scaffold which did not show any cytotoxic effects and preserved the cell viability *in vitro*. GS-Hyd also promoted cell adhesion and proliferation. Considering the fact that cells were round shaped at the day of seeding (not shown) but could expand their elongations and obtained a fibroblast-like appearance within 24 h (Figure 4), we conclude that MSCs very well adhere to the GS-Hyd scaffold. Moreover, the fact that more cells were visible on the scaffolds at day 7 than day 2 post seeding and the observation that the MSCs had formed colonies after 7 days of cell seeding indicate that the GS-Hyd complex supports cell proliferation (Figures 3, 4 and 5). The interconnected pores of the scaffold may further promote cellular adherence. Additionally, the pore size (1–2 μm) of the scaffolds seems to be large enough to allow medium flow which would provide ideal conditions for cell proliferation on the scaffolds.

The composition of the scaffold and the speed of scaffold degradation in its biological environment, are important factors for their applicability *in vivo*. However, this is not the case for GS-Hyd scaffold, because its rate of degradation can be manipulated during the synthesis. In previous studies on similar scaffolds, they were kept in the body of rats for 30–90 days after surgery.^{64,65} In our study, we implanted and kept the scaffolds for 21 days. During this period, the speed of scaffold

degradation was much higher shortly after implantation than at later times. This could be explained by the fact that gelatin, the main component of the scaffold, is easily degraded and could hence account for the major weight lost observed in the beginning. However, additional experiments are required to identify the cause(s) for the large loss in scaffold weight early after *in vivo* implantation. At 21 days after implantation about 30% of the initial weight of the scaffolds remained. The SEM analyses revealed that the loss of scaffold weight is accompanied by the disappearance of the interconnections between pores inside the scaffold which suggests a direct link between compound degradation and inter-junction loss. Structural degradation rates at the three examined anatomical sites proved that the degradative capacities are tissue-specific and according to our SEM micrographs the thigh muscle has the highest capacity for the scaffold degradation. During the whole *in vivo* study, the rats did not display any signs of scaffold-related toxicity, other than a mild inflammation.

In conclusion, this study showed that GS-Hyd scaffolds are degraded *in vivo* at rates compatible with their application in tissue engineering. It was also shown that GS-Hyd did not have any cytotoxic effects and also could promote cell adhesion and proliferation *in vitro*, but to reach to a definite conclusion about the toxic effects of the scaffold *in vivo*, further experiments are needed. Therefore, we suggest that GS-Hyd scaffolds can be used for tissue engineering, but still more assays and *in vivo* studies are required to investigate other characteristics of this scaffold which are important for its clinical use.

Acknowledgments

This work was partly supported by grant Sci-1385-21145 from Ferdowsi University of Mashhad, Iran and the GS-Hyd scaffold was filed as a patent (Number 51213).

References

1. Fuchs JR, Nasser BA, Vacanti JP. Tissue engineering: a 21st century solution to surgical reconstruction. *Ann Thorac Surg.* 2001;72:577-591.
2. Langer R, Vacanti JP. Tissue engineering. *Science.* 1993;260:920-926.
3. Nerem RM, Sambanis A. Tissue engineering: from biology to biological substitutes. *Tissue Eng.* 1995;1:3-13.
4. Kim KM, Evans GRD. Tissue engineering: The future of stem cells. In: Ashammakhi N, Reis RL, eds. *Topics in tissue engineering.* USA; 2005:1-21.
5. Katz AJ, Lull R, Hedrick MH, Futrell JW. Emerging approaches to the tissue engineering of fat. *Clin Plast Surg.* 1999;26:587-603.
6. Stock UA, Vacanti JP. Tissue engineering: current state and prospects. *Annu Rev Med.* 2001;52:443-451.
7. Robert L. Matrix biology: past, present and future. *Pathol Biol (Paris).* 2001;49:279-283.
8. Rahaman MN, Mao JJ. Stem cell-based composite tissue constructs for regenerative medicine. *Biotechnol Bioeng.* 2005;91:261-284.
9. Choi YS, Park SN, Suh H. Adipose tissue engineering using mesenchymal stem cells attached to injectable PLGA spheres. *Biomaterials.* 2005;26:5855-5863.
10. Ifkovits JL, Wu K, Mauck RL, Burdick JA. The influence of fibrous elastomer structure and porosity on matrix organization. *PLoS One.* 2010;5:e15717.
11. Soliman S, Sant S, Nichol JW, Khabiry M, Traversa E, Khademhosseini A. Controlling the porosity of fibrous scaffolds by modulating the fiber diameter and packing density. *J Biomed Mater Res A.* 2011;96:566-574.
12. Heller J, Sparer RV, Zentner GM. Poly (ortho esters). In: Chasin M LR, ed. *Biodegradable polymers as drug delivery systems.* New York: Marcel Dekker; 1990:121-161.
13. Agrawal CM, Ray RB. Biodegradable polymeric scaffolds for musculoskeletal tissue engineering. *J Biomed Mater Res.* 2001;55:141-150.
14. Ishaug SL, Crane GM, Miller MJ, Yasko AW, Yaszemski MJ, Mikos AG. Bone formation by three-dimensional stromal osteoblast culture in biodegradable polymer scaffolds. *J Biomed Mater Res.* 1997;36:17-28.

15. Lowry KJ, Hamson KR, Bear L, Peng YB, Calaluce R, Evans ML, Anglen JO, Allen WC. Polycaprolactone/glass bioabsorbable implant in a rabbit humerus fracture model. *J Biomed Mater Res.* 1997;36:536-541.
16. Niklason LE, Gao J, Abbott WM, Hirschi KK, Houser S, Marini R, Langer R. Functional arteries grown *in vitro*. *Science.* 1999;284:489-493.
17. Freed LE, Vunjak-Novakovic G, Biron RJ, Eagles DB, Lesnoy DC, Barlow SK, Langer R. Biodegradable polymer scaffolds for tissue engineering. *Biotechnology (N Y).* 1994;12:689-693.
18. Takahara A, Coury AJ, Hergenrother RW, Cooper SL. Effect of soft segment chemistry on the biostability of segmented polyurethanes. I. *In vitro* oxidation. *J Biomed Mater Res.* 1991;25:341-356.
19. Kim BS, Mooney DJ. Development of biocompatible synthetic extracellular matrices for tissue engineering. *Trends Biotechnol.* 1998;16:224-230.
20. Peter SJ, Miller MJ, Yasko AW, Yaszemski MJ, Mikos AG. Polymer concepts in tissue engineering. *J Biomed Mater Res.* 1998;43:422-427.
21. Dorozhkin SV, Epple M. Biological and medical significance of calcium phosphates. *Angew Chem Int Ed Engl.* 2002;41:3130-3146.
22. Roseberry HH, Hastings AB, Morse JK. X-ray analysis of bone and teeth. *J Biol Chem.* 1931;90:395-407.
23. Klein CP, de Blicq-Hogervorst JM, Wolke JG, de Groot K. Studies of the solubility of different calcium phosphate ceramic particles *in vitro*. *Biomaterials.* 1990;11:509-512.
24. Daculsi G. Biphasic calcium phosphate concept applied to artificial bone, implant coating and injectable bone substitute. *Biomaterials.* 1998;19:1473-1478.
25. LeGeros RZ, Lin S, Rohanizadeh R, Mijares D, LeGeros JP. Biphasic calcium phosphate bioceramics: preparation, properties and applications. *J Mater Sci Mater Med.* 2003;14:201-209.
26. Pasteris JD, Wopenka B, Freeman JJ, Rogers K, Valsami-Jones E, van der Houwen JA, Silva MJ. Lack of OH in nanocrystalline apatite as a function of degree of atomic order: implications for bone and biomaterials. *Biomaterials.* 2004;25:229-238.
27. Koerten HK, van der Meulen J. Degradation of calcium phosphate ceramics. *J Biomed Mater Res.* 1999;44:78-86.

28. Horvath L, Smit I, Sikiric M, Filipovic-Vincekovic N. Effect of cationic surfactant on the transformation of octacalcium phosphate. *J Cryst Growth*. 2000;219:91-97.
29. Koumoulidis GC, Katsoulidis AP, Ladavos AK, Pomonis PJ, Trapalis CC, Sdoukos AT, Vaimakis TC. Preparation of hydroxyapatite via microemulsion route. *J Colloid Interface Sci*. 2003;259:254-260.
30. Sarda S, Heughebaert M, Lebugle A. Influence of the type of surfactant on the formation of calcium phosphate in organized molecular systems. *Chem Mater*. 1999;11:2722-2727.
31. Yan L, Li Y, Deng ZX, Zhuang J, Sun X. Surfactant-assisted hydrothermal synthesis of hydroxyapatite nanorods. *Int J Inorg Mater*. 2001;3:633-637.
32. Yao J, Tjandra W, Chen YZ, Tam KC, Ma J, Soh B. Hydroxyapatite nanostructure material derived using cationic surfactant as a template. *J Mater Chem*. 2003;13:3053-3057.
33. Phan PV, Grzanna M, Chu J, Polotsky A, el-Ghannam A, Van Heerden D, Hungerford DS, Frondoza CG. The effect of silica-containing calcium-phosphate particles on human osteoblasts *in vitro*. *J Biomed Mater Res A*. 2003;67:1001-1008.
34. Porter AE, Best SM, Bonfield W. Ultrastructural comparison of hydroxyapatite and silicon-substituted hydroxyapatite for biomedical applications. *J Biomed Mater Res A*. 2004;68:133-141.
35. Kokubo T, Kim HM, Kawashita M. Novel bioactive materials with different mechanical properties. *Biomaterials*. 2003;24:2161-2175.
36. Ohtsuki C, Kokubo T, Yamamuro T. Mechanism of apatite formation on CaOsingle bondSiO2single bondP2O5 glasses in a simulated body fluid. *J Non-Cryst Solids*. 1992;143.
37. Hench LL. Bioceramics: from concept to clinic. *J Am Ceram Soc*. 1991;74:1487-1510.
38. Hench LL, Splinter RJ, Allen WC, Greenlee TK. Bonding mechanisms at the interface of ceramic prosthetic materials. *J Biomed Mater Res* 1971;5:117-141.
39. Krikorian V, Pochan DJ. Poly (l-lactic acid)/layered silicate nanocomposite: fabrication, characterization, and properties. *Chem Mater*. 2003;15:4317-4324.

40. Villacampa AI, Garcia-Ruiz JM. Synthesis of a new hydroxyapatite-silica composite material. *J Cryst Growth*. 2000;211:111-115.
41. Kang HW, Tabata Y, Ikada Y. Fabrication of porous gelatin scaffolds for tissue engineering. *Biomaterials*. 1999;20:1339-1344.
42. TenHuisen KS, Brown PW. The formation of hydroxyapatite-gelatin composites at 38 degrees C. *J Biomed Mater Res*. 1994;28:27-33.
43. Ren L, Tasura S, Hayakawa A. Synthesis and characterization of gelatin-siloxane hybrids derived through solgel procedure. *Chem Mater Sci*. 2001;21:115-121.
44. Silva TS, Primo BT, Silva Junior AN, Machado DC, Viezzer C, Santos LA. Use of calcium phosphate cement scaffolds for bone tissue engineering: *In vitro* study. *Acta Cir Bras*. 2011;26:7-11.
45. Koh CJ, Atala A. Therapeutic cloning and tissue engineering. *Curr Top Dev Biol*. 2004;60:1-15.
46. Naughton GK. From lab bench to market: critical issues in tissue engineering. *Ann N Y Acad Sci*. 2002;961:372-385.
47. Van Eijk F, Saris DB, Riesle J, Willems WJ, Van Blitterswijk CA, Verbout AJ, Dhert WJ. Tissue engineering of ligaments: A comparison of bone marrow stromal cells, anterior cruciate ligament, and skin fibroblasts as cell source. *Tissue Eng*. 2004;10:893-903.
48. Pittenger MF, Mackay AM, Beck SC, Jaiswal RK, Douglas R, Mosca JD, Moorman MA, Simonetti DW, Craig S, Marshak DR. Multilineage potential of adult human mesenchymal stem cells. *Science*. 1999;284:143-147.
49. Colter DC, Class R, DiGirolamo CM, Prockop DJ. Rapid expansion of recycling stem cells in cultures of plastic-adherent cells from human bone marrow. *Proc Natl Acad Sci U S A*. 2000;97:3213-3218.
50. Jiang Y, Jahagirdar BN, Reinhardt RL, Schwartz RE, Keene CD, Ortiz-Gonzalez XR, Reyes M, Lenvik T, Lund T, Blackstad M, Du J, Aldrich S, Lisberg A, Low WC, Largaespada DA, Verfaillie CM. Pluripotency of mesenchymal stem cells derived from adult marrow. *Nature*. 2002;418:41-49.
51. Amin EM, Reza BA, Morteza BR, Maryam MM, Ali M, Zeinab N. Microanatomical evidences for potential of mesenchymal stem cells in amelioration of striatal degeneration. *Neurol Res*. 2008;30:1086-1090.

52. Bruder SP, Jaiswal N, Ricalton NS, Mosca JD, Kraus KH, Kadiyala S. Mesenchymal stem cells in osteobiology and applied bone regeneration. *Clin Orthop Relat Res.* 1998:S247-256.
53. Fan H, Hu Y, Zhang C, Li X, Lv R, Qin L, Zhu R. Cartilage regeneration using mesenchymal stem cells and a PLGA-gelatin/chondroitin/hyaluronate hybrid scaffold. *Biomaterials.* 2006;27:4573-4580.
54. Ouyang HW, Goh JC, Thambyah A, Teoh SH, Lee EH. Knitted poly-lactide-co-glycolide scaffold loaded with bone marrow stromal cells in repair and regeneration of rabbit achilles tendon. *Tissue Eng.* 2003;9:431-439.
55. Ge Z, Goh JC, Lee EH. The effects of bone marrow-derived mesenchymal stem cells and fascia wrap application to anterior cruciate ligament tissue engineering. *Cell Transplant.* 2005;14:763-773.
56. Edalatmanesh MA, Matin MM, Neshati Z, Bahrami AR, Kheirabadi M. Systemic transplantation of mesenchymal stem cells can reduce cognitive and motor deficits in rats with unilateral lesions of the neostriatum. *Neurol Res.* 2010;32:166-172.
57. Neshati Z, Matin MM, Bahrami AR, Moghimi A. Differentiation of mesenchymal stem cells to insulin-producing cells and their impact on type 1 diabetic rats. *J Physiol Biochem.* 2010;66:181-187.
58. Xie H, Yang F, Deng L, Luo J, Qin T, Li X, Zhou GQ, Yang Z. The performance of a bone-derived scaffold material in the repair of critical bone defects in a rhesus monkey model. *Biomaterials.* 2007;28:3314-3324.
59. Liu H, Fan H, Toh SL, Goh JC. A comparison of rabbit mesenchymal stem cells and anterior cruciate ligament fibroblasts responses on combined silk scaffolds. *Biomaterials.* 2008;29:1443-1453.
60. Arnhold S, Klein H, Semkova I, Addicks K, Schraermeyer U. Neurally selected embryonic stem cells induce tumor formation after long-term survival following engraftment into the subretinal space. *Invest Ophthalmol Vis Sci.* 2004;45:4251-4255.
61. Tang DQ, Cao LZ, Burkhardt BR, Xia CQ, Litherland SA, Atkinson MA, Yang LJ. *In vivo* and *in vitro* characterization of insulin-producing cells obtained from murine bone marrow. *Diabetes.* 2004;53:1721-1732.

62. Lakard S, Herlem G, Propper A, Kastner A, Michel G, Valles-Villarreal N, Gharbi T, Fahys B. Adhesion and proliferation of cells on new polymers modified biomaterials. *Bioelectrochemistry*. 2004;62:19-27.
63. Thiery JP. Cell adhesion in development: a complex signaling network. *Curr Opin Genet Dev*. 2003;13:365-371.
64. Piao H, Kwon JS, Piao S, Sohn JH, Lee YS, Bae JW, Hwang KK, Kim DW, Jeon O, Kim BS, Park YB, Cho MC. Effects of cardiac patches engineered with bone marrow-derived mononuclear cells and PGCL scaffolds in a rat myocardial infarction model. *Biomaterials*. 2007;28:641-649.
65. Kim M, Choi YS, Yang SH, Hong HN, Cho SW, Cha SM, Pak JH, Kim CW, Kwon SW, Park CJ. Muscle regeneration by adipose tissue-derived adult stem cells attached to injectable PLGA spheres. *Biochem Biophys Res Commun*. 2006;348:386-392.

